buildings

MDPI

Article

Computational Aerodynamic Optimization of Wind-Sensitive Irregular Tall Buildings

Fadi Alkhatib [1], Narimah Kasim [2], Wan Inn Goh [1], Nasir Shafiq [3], Mugahed Amran [4,5,*], Evgenii Vladimirovich Kotov [6] and Mohammed Abdo Albaom [7]

[1] Department of Structural Engineering, Faculty of Civil Engineering and Built Environment, Universiti Tun Hussein Onn Malaysia (UTHM), Parit Raja, Batu Pahat 86400, Johor, Malaysia; alkhatibfadi90@gmail.com (F.A.); wigoh@uthm.edu.my (W.I.G.)
[2] Faculty of Technology Management & Business, Universiti Tun Hussein Onn Malaysia (UTHM), Parit Raja, Batu Pahat 86400, Johor, Malaysia; narimah@uthm.edu.my
[3] Department of Civil and Environmental Engineering, Faculty of Engineering, Universiti Teknologi PETRONAS, Seri Iskandar 32610, Perak, Malaysia; nasirshafiq@utp.edu.my
[4] Department of Civil Engineering, College of Engineering, Prince Sattam Bin Abdulaziz University, Alkharj 16273, Saudi Arabia
[5] Department of Civil Engineering, Faculty of Engineering and IT, Amran University, Amran 9677, Yemen
[6] Peter the Great St. Petersburg Polytechnic University, 195251 St. Petersburg, Russia; ekotov.cfd@gmail.com
[7] Department of Computer Science, Faculty of Computer Science and Information Technology, Universiti Pura Malaysia (UPM), Serdang 43400, Selangor, Malaysia; mohammedabdo773@gmail.com
* Correspondence: m.amran@psau.edu.sa

Abstract: Wind-induced loads and motions play a critical role in designing tall buildings and their lateral structural systems. Building configuration represented by its outer shape is a key parameter in determining these loads and structural responses. However, contemporary architecture trends towards creating taller buildings with more complex geometrical shapes to offer unique designs that become a signature on the map of the world. As a result, evaluating wind-induced motions on such structures becomes more challenging to be evaluated and predicted. This paper presents a computational performance-based aerodynamic optimization with minor imposed modifications that have little to no impact on architectural and structural design intent. The developed tool aims to assist both architects and engineers to seek a sustainable optimal design decision at the early stage of design by employing different computational technological tools in an automated manner. A computational optimization methodology consisting of a computational fluid dynamic coupled with finite element analysis and embedded within a radial basis function surrogate model is proposed to mitigate wind-induced loads on tall buildings. In addition, a numerical example implementing the proposed methodology on selected case study is presented and discussed. The proposed approach was able to achieve a minimization of 13.83% and 23.12% for along-wind and across-wind loads, respectively, which is translated to a reduction in structural response by 12.95% and 14.31% in maximum deflection for along-wind and across-wind directions, respectively.

Keywords: tall buildings; CFD; optimization; wind loads

Citation: Alkhatib, F.; Kasim, N.; Goh, W.I.; Shafiq, N.; Amran, M.; Kotov, E.V.; Albaom, M.A. Computational Aerodynamic Optimization of Wind-Sensitive Irregular Tall Buildings. *Buildings* **2022**, *12*, 939. https://doi.org/10.3390/buildings12070939

Academic Editors: Bo Chen, Ying Sun and Min Liu

Received: 17 May 2022
Accepted: 30 June 2022
Published: 2 July 2022

1. Introduction

The idea of vertical habitation is not new and has been a trend propelled for decades by the growth of cities and the resulting overpopulation. The 16th century Yemeni city of Shibam, which is considered to have the first skyscrapers in the history [1], is a living example, with mud brick tower buildings of five to eight floors heigh intended to stave off Bedouin raids. In the late 19th century, new high-rise buildings started to emerge in the North American cities due to social, economic, and technological development. Currently, modern architectures are characterized by their irregular shapes, and tall buildings are becoming taller with complex geometrical forms [2]. As a result, designing and optimizing

tall buildings becomes a challenging task, and compounds the problem of collaboration between architects and engineers [3], where both strive to fulfil different requirements but mutual cost-effective sustainable design outputs.

More importantly, tall buildings are sensitive structures to lateral loads such as wind and earthquakes. Nevertheless, while designing for earthquakes, it is essential to lower the structure's mass and gravity loads in order to control the inertial forces generated by an earthquake [4]. Applying this will further increase the wind-induced motions and loads on tall buildings to such an extent that it becomes a challenge to meet strength and serviceability design criteria. Thus, wind loads normally dictate the development process of tall buildings and govern the design and optimization of their lateral structural system [4].

One controlling parameter of wind-induced loads and their respective structural responses is the geometrical form representing the exterior shape of the building [5]. Especially for complex shapes, it is almost impossible to standardize the wind loads on buildings. That is demonstrated by the limited shapes, rectangular and circular, in design codes' available approaches of computing wind loads on structures, such as the equivalent static wind load method (ESWL). Evaluating wind actions on a building is therefore carried out by physical wind tunnel tests or computational fluid dynamics (CFD) numerical simulation. However, this opens a wide opportunity in manipulating wind loads and motions on structures by altering their geometrical forms, either globally or locally [5]. Changes in wind loads are thus proportionate to the changes imposed on buildings' geometries. Global modifications entail major alterations to the building form, either horizontally or vertically, such as setback, tapering, and twisting. On the contrary, introducing local modifications will have minor impacts on the building architecturally and structurally, yet still have an influence on the generated wind loads and structural response that can be optimized to a certain extent.

Several numerical and experimental studies have investigated the effect of global (major) and local (minor) modifications on tall building wind responses. Considering major modifications, different building plan configurations showed a strong relation to wind structural responses [6–10]. Hayashida et al. [6] studied multiple building plan configuration to examine wind-induced dynamic response of building and found that triangular and 'Y'-shaped building plans counter smaller responses of structural displacement in comparison to rectangular plans. Building dimension and ratio of buildings' height to width and thickness also has a significant influence on wind distribution and characteristics, as suggested by Mou et al. [9]. Applying horizontal limps in building plans as studied by [10] showed to be effective in minimizing external wind pressure on building faces. Tapering and setback are amongst the popular major aerodynamic modifications in tall buildings to lessen wind responses. Tapering has a significant impact on mitigating across-wind responses over along-wind responses [11–13]; however, Kim et al. [12] stipulated through examining different tapering models with different structural damping ratios that increases in tapering may result in an adverse effect by maximizing across-wind displacement responses. Similar to tapering, setback was also found to be an effective approach, especially for lessening across-wind response [13]. However, Bairagi and Dalui [14] investigated the effect of building configuration for wind distribution on square and setback building forms, and the setback form developed an excessive suction pressure at the top of the roof in comparison to the square model. Another study by the same authors [15] investigated the impact of single-side and both-side setback, where the latter was noticed to be more susceptible to wind motions. Large openings and through-building gaps were also considered among major modification options due to its effectiveness in reducing across-wind excitation as a result of the organized or narrow-band vortex-shedding process [16]. Moreover, such modification can be exploited to maximize local wind resources, as explored by Ruiz et al. [17], where fillet radius and duct diameter parameters of the opening are investigated in enhancing the magnitude and uniformity of wind speed with a ratio of 0.2 providing the best opening configuration.

Minor modification, with corner configuration being the common type, is a key parameter in manipulating wind responses on tall buildings, where imposing slight modifications on building corners can result in drastic changes in aerodynamic characteristics such as drag, which has a possibility of decreasing up to 60% from the original value according to Tamura et al. [18]. However, when dealing with minor corner modification, the angle of attack (AOA) attributed to wind direction is a key contributor to the effectiveness of the imposed modifications, as demonstrated by a rectangular building shape case study by Miyashita et al. [19], where no significant impact was recorded for wind blow angles less than 5 degrees. Corner rounding, chamfering, and recession are amongst popular kinds of tall building aerodynamic corner configurations that have been investigated by multiple studies and proved to be effective in mitigating both along-wind and across-wind responses [20–26]. Elshaer et al. [4] established that these types of modifications contribute to the lessening of both wind drag and lift forces on tall buildings. Nonetheless, Li et al. [24] found that chamfered corners are more potent in reducing drag forces and recessed corners show similar effectiveness in reducing lift forces, where Mandal et al., on the other hand, concluded that rounded corners outperform chamfered in both. Other corner modifications including slotting, fins, and corner-cut are also examined in other studies [27–29], and showed similar strong correlations to wind responses on tall buildings. However, Kwok and Baily [27] established that slotted corners effectively mitigate both along-wind and across-wind responses, while fins only help to reduce across-wind response.

Combining major and minor modifications in a single model is another approach that was explored by multiple studies [30–34]. In fact, Tanaka et al. [31] asserted that incorporating these modifications is essential to develop a comprehensive understanding of aerodynamic characteristics of tall buildings with different configurations. Meanwhile, Tamura et al. [32] concluded that composite models with combined modifications showed better aerodynamic performance in terms of force and pressure measurements in comparison to a single modification. Ultimately, although most of these researchers carried out their investigations based on regular rectangular or square building plans, such modifications are also applicable with similar effects for irregular building forms, as implemented in recent studies by Mandal et al. [26] on a U-shaped plan and Sanyal et al. [29] on a Y-shaped plan. A summary of previous similar studies is summarized in Table 1.

Building on these fascinating and comprehensive aerodynamic optimization studies as benchmarks, this study presents a new performance-based aerodynamic optimization approach. This is achieved by performing computational fluid dynamics (CFD) that is integrated in a parametrical environment and connected to finite element analysis software for structural response assessment. A radical basis function (RBF)-surrogate-based model is then utilized to create a dataset to be trained, and a final functional response is constructed within the pre-defined design domain to generate an aerodynamic building form based on defined optimal design parameters. In contrast to previous studies, where the focus was on understanding the effect of specific aerodynamic modifications to particular building forms, and because in real life tall building configurations are trending towards complex shapes and vertical irregularity, the novelty of this study lies in adopting a flexible computational approach that can be utilized in industrial practice for aerodynamic optimization of tall buildings with independent applicability for different complex geometrical forms. Moreover, this research extends the application of the performance-based wind design of tall buildings, which, unlike seismic engineering, has not been sufficiently explored and adopted in wind engineering [35].

The paper is structured into three sections. Section 1 (this section) describes the topic under investigation and summarizes the related studies within a similar scope. In Section 2, a CFD validation study is conducted to verify the reliability and accuracy of the proposed CFD model in comparison to real physical BLWT. Section 3 describes the developed optimization methodology, while Section 4 demonstrates its effectiveness through a real case study example wherein the results and discussion are presented. Finally, in Section 5 conclusions and further recommendations are drawn.

Table 1. Literature review summary.

No	Author	Year	Method	Class	Modification	Approach/Aim
1	Kwok and Bailey [27]	1987	BLWT	Minor	Slotted corners, fins, vented fins	Investigating the impact of aerodynamic devices on wind-induced responses of tall buildings.
2	Kwok [20]	1988	BLWT	Minor	Chamfering corners, slotting corners	Measuring mean wind displacement response.
3	Hayashida and Iwasa [6]	1990	BLWT	Major	Circular, triangular, and Y-shaped layout plan	Evaluating aerodynamic effect on dynamic response behavior of buildings.
4	Dutton and Isyumov [16]	1990	BLWT	Major	Opening	Evaluating wind response and building forces based on high-frequency force balance technique.
5	Miyashita et al. [19]	1993	BLWT	Minor	Chamfering corners, opening	Evaluating wind-induced building response through modal analysis.
6	Tamura et al. [18]	1998	CFD	Minor	Chamfering corners, rounding corners	Evaluating aerodynamic characteristics such as Reynolds number and fluctuation of drag and lift forces.
7	Tamura and Miyagi [21]	1999	BLWT	Minor	Corner chamfering, corner rounding	Measuring of aerodynamic quantities, such as averaged and fluctuating statistics of lift and drag forces.
8	Kim and You [11]	2002	BLWT	Major	Tapering	Evaluating mean and RMS-force coefficients and power spectral density functions.
9	Gu and Quan [30]	2004	BLWT	Major/Minor	Square and rectangular plan, with corner chamfering and recession	Evaluating across-wind dynamic forces based on high-frequency force balance technique.
10	Kim et al. [12]	2008	BLWT	Major	Tapering	Investigating the reduction in RMS across-wind displacement responses.
11	Tse et al. [22]	2009	BLWT	Minor	Corner chamfering, corner recessions	Evaluating wind forces using high-frequency force balance technique for building models.
12	Zhengwei et al. [23]	2012	BLWT	Minor	Corner recessions	Analyzing mean and RMS coefficients of the aerodynamic base moment and torque.
13	Tanaka et al. [31]	2012	BLWT	Major/Minor	Twisting, opening, helical, corner chamfering, corner recessions	Investigating aerodynamic wind forces and wind pressures based on high-frequency force balance technique.
14	Tamura et al. [32]	2013	CFD	Major/Minor	Cross-section configurations	Investigating variations in peak pressures, aerodynamic and response characteristics, wind load combination effects, and flow field characteristics.
15	Xie [13]	2014	BLWT	Major	Tapering, twisting, stepping	Measuring dynamic force coefficient using power spectra approach.
16	Kim et al. [7]	2014	BLWT	Major	Atypical building shapes	Comparing wind load effects by conducting time history analysis.

Table 1. *Cont.*

No	Author	Year	Method	Class	Modification	Approach/Aim
17	Bhattacharyya et al. [8]	2014	CFD	Major	E-shaped building plan	Evaluating mean pressure coefficient of all building faces.
18	Mou et al. [9]	2017	CFD	Major	Building dimension variations	Investigating wind pressure distribution due to dimension ratio alteration.
19	Elshaer et al. [4]	2017	CFD	Minor	Corner configuration	Optimizing mean drag coefficient and standard deviation.
20	Bairagi and Dalui [15]	2018	CFD	Major	Single setback, double setback	Evaluating pressure, forces, and torsional moment coefficients.
21	Li et al. [24]	2018	BLWT	Minor	Corner configuration	Evaluating mean wind pressure coefficients, base moment coefficients, local wind force coefficients, power spectral densities, and vertical correlation coefficients.
22	Daemei et al. [33]	2019	CFD	Major/Minor	Tapering, setback, helical, chamfering, recession, rounding	Assessing aerodynamic efficiency behavior of along-wind responses based on drag coefficient.
23	Thordal et al. [25]	2020	CFD	Minor	Corner chamfering, corner rounding	Investigating surface pressure distribution, peak predicted structural responses, and floor loadings.
24	Bairagi and Dalui [14]	2020	CFD	Major	Setback	Measuring wind pressure distribution around building.
25	Mandal et al. [26]	2021	CFD	Minor	Corner chamfering and corner rounding on U-shaped building plan	Exploring wind resistance design parameters of force coefficient and pressure coefficients.
26	Ruiz et al. [17]	2021	CFD	Major	Opening (diameter and fillet radius)	Evaluating magnitude and uniformity of the wind speed and optimizing turbulent kinetic energy.
27	Assainar and Dalui [34]	2021	CFD	Major/Minor	Pentagonal plan with corner configuration, setback, and tapering forms	Evaluating forces and pressure coefficients and investigating structural dynamic behavior of building.
28	Paul and Dalui [10]	2021	CFD	Major	Horizontal limps on building plan	Evaluating the external pressure coefficients on building faces.
29	Gaur and Raj [28]	2022	CFD	Minor	Corner-cut configuration	Evaluating force coefficients, base moments, power spectra, external surface pressure coefficients, and flow field characteristics.
30	Sanyal and Dalui [29]	2022	CFD	Minor	Corner-cut on Y-shaped plan	Evaluating wind-induced force, moment, and torsional coefficients.

2. Research Methodology

The development of research procedures of this work started by conducting a CFD validation study to adopt the appropriate CFD model for an outdoor airflow analysis of a building with its correspondent parameters including turbulence model and mesh sizes. Consequently, aerodynamic optimization procedures were developed and integrated into a flowchart that can be implemented to any desired case study.

2.1. CFD Validation

Validation study was carried out to evaluate the accuracy and liability of the adopted CFD analysis and its numerical findings in comparison to real physical BWLT prior to integrating it into the optimization cycle. The Commonwealth Advisory Aeronautical Research Council (CAARC) Standard Tall Building Model, a building constructed in 1969 to be a reference for wind tunnel testing [36] and its use, has now been broadened to include CFD analysis and verification [37], and was utilized in the validation process. A TJ University wind tunnel test output with 0° wind direction in Meng et al.'s [37] study was selected as the reference to perform the sensitivity analysis and evaluate the mean wind pressure coefficient (C_p) of the proposed CFD. Upon verifying the accuracy of the CFD analysis, different mesh resolutions were evaluated against accuracy and time to find an appropriate model maintaining the required accuracy within less computational time.

Nevertheless, to establish an effective numerical model, several factors and settings were considered. In the first place, a minimum blockage ratio of 5% should be met during the computational setting based on the following relation:

$$\delta = \frac{A_0}{A}$$

where δ is the blockage ration, A_0 is the building wall area perpendicular to wind direction, and A is the area of computational domain perpendicular to the wind direction. The Outflow boundary condition was employed to simulate steady and incompressible wind flow. Wall boundary conditions were used to describe the wall of the computational domain and the surface of the tall CAARC standard building [37]. SIMPLE pressure–velocity coupling algorithms were adopted for solver setting, and the Second-Order Upwind Scheme was adopted to discretize momentum, turbulent kinetic energy, and turbulence dissipation rate. Finally, convergence of simulation is assumed to be reached when residuals of x, y, z momentum, k, ε, and continuity are less than 10^{-3}, as recommended by Frank et al. [38]. The processor used for this study is an intel (R) Core (TM) i7-10750H CPU @ 2.60 GHz, 32.0 GB RAM, running in parallel decomposition.

2.2. CAARC Building Assembly

The CAARC standard building was replicated in a rectangular building model having similar dimensions of 30.48 m, 45.72 m, and 182.88 m for length, width, and height, respectively. Twenty wind pressure taps were generated and situated at 2/3 height of the building corresponding to 121.92 m from the ground, with five taps at each face of the building, as shown in Figure 1. Consequently, the wind pressure coefficient C_p was measured for these taps in relation to a benchmark static point situated at the flow inlet within the center of the building x-axis and at the relevant height of the building.

The computational domain of the tunnel was duplicated to match the one from the reference paper with the corresponding dimensions of 900 m, 600 m, and 400 m for length, width, and height, respectively, as shown in Figure 2. The building is situated at the central line of the tunnel x-axis and within 300 m from the inlet point of flow to provide sufficient space for the air flow to be fully developed within an allowable calculated blockage ratio of 3.4%, below the recommended threshold of 5% [9,39].

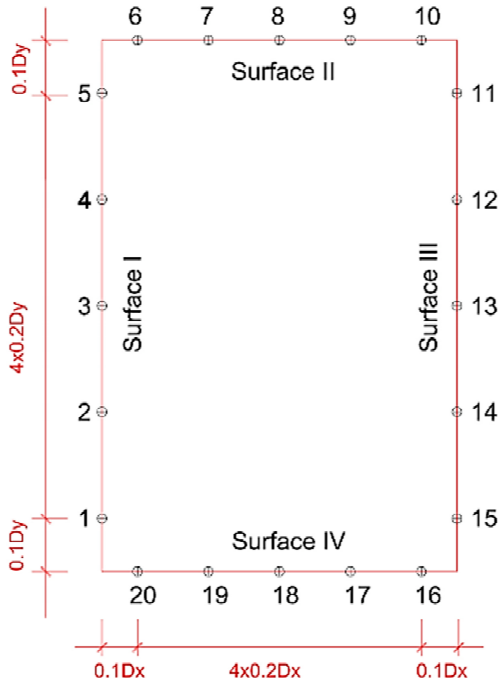

Figure 1. Pressure taps on CAARC building faces.

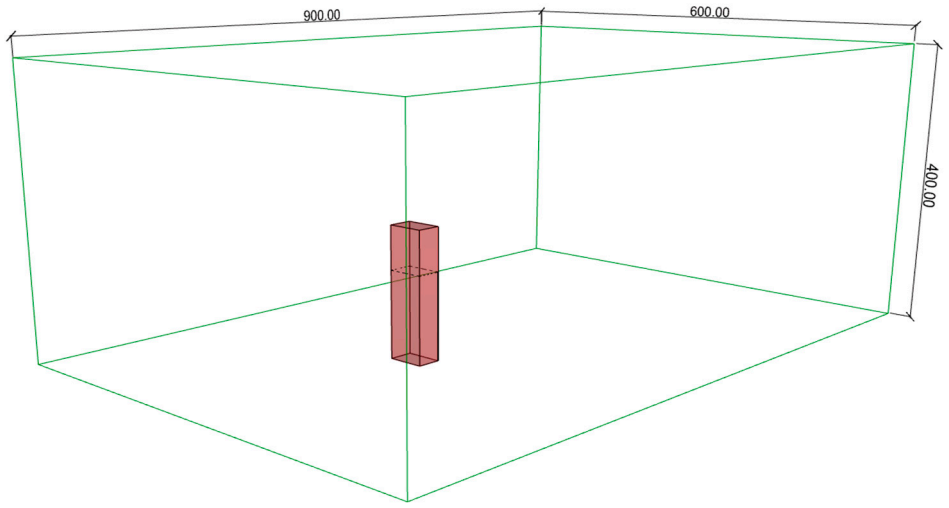

Figure 2. Wind tunnel domain.

2.3. Turbulence Models

Three turbulence models were investigated for their impact on wind pressure coefficients in comparison to TJ experimental results: standard $k-\varepsilon$, RNG $(k-\varepsilon)$, and realizable $(k-\varepsilon)$. During the evaluation of turbulence models other parameters remained constant, including wind profile and wind speed. For each tested model, wall function was employed to satisfy the physics in the near wall zone by encompassing the inner region between the wall and the turbulence fully developed region. Mesh size was also set constantly for the three models with a maximum grid size of 0.00054 H [37] corresponding to 0.98755 m with cell numbers equal to 678,600. This grid setting was adopted for this section; however, for identifying the sensitivity of the wind pressure coefficient to different grid resolutions, cell sizes and numbers were adjusted for further comparison in the next section. The threshold of residuals' convergence was set to 0.0001 as recommended by Frank et al. [38] to limit iteration numbers within an acceptable computational time.

The results of the three analyzed models are plotted in Figure 3. Although it is observed that all models simulate a similar pattern with agreement to TJ experimental values,

demonstrating a good accuracy of the numerical outputs, the RNG $(k-\varepsilon)$ turbulence model showed the best agreement for all distributed pressure taps followed by the realizable $(k-\varepsilon)$, and eventually the least agreed model was the standard. Absolute deviation for all four surfaces representing the faces of the building and their attached pressure taps for the three adopted models was calculated and illustrated in Figure 4. The lowest median absolute deviation for all surfaces was best achieved at 6.07% for the RNG model, whereas 17% and 26% are the computed median absolute deviation for the realizable and standard models, respectively.

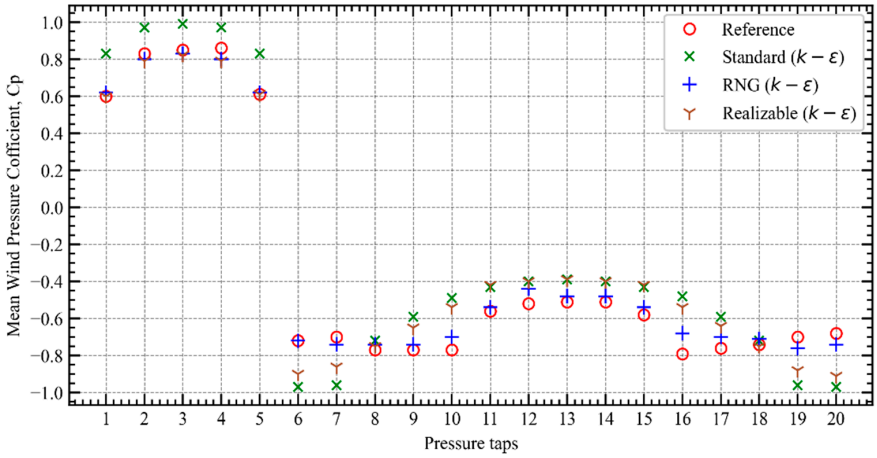

Figure 3. C_p values for different turbulence models.

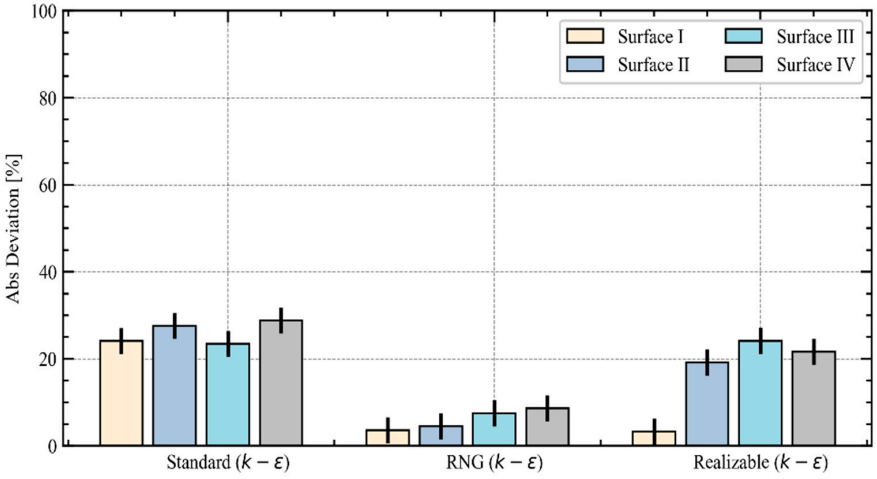

Figure 4. Comparison of numerical C_p values in each building surface (face) to the experimental reference.

2.4. Mesh Resolutions

Mesh grid size and numbers were evaluated to study the responsiveness of the wind pressure coefficient against different mesh resolutions and based on the RNG $(k-\varepsilon)$ turbulence model that was tested in Section 2.4. Three different meshing generations, namely coarse, medium, and fine, shown in Figure 5, were investigated in terms of result accuracy and computational time. Mesh sizes were determined based on Frank et al.'s [38] recommendation for CFD simulation guidelines, where meshing grid size is firstly obtained by dividing the shortest width of the building by 10. The resulting size then can be multiplied by $\sqrt{2}$ nth times for nth refinement required. Three mesh types were evaluated, as described in Table 2.

B in Table 2 indicates the shortest width of the building. Although all three mesh sizes generated similar deviations to the reference study as stipulated in Figure 6, there was a significant difference in computational times, which has an impact for running such

simulations for the number of iterations required. Based on the result, the medium mesh was adopted, as it has similar accuracy but better time performance in comparison to fine ones.

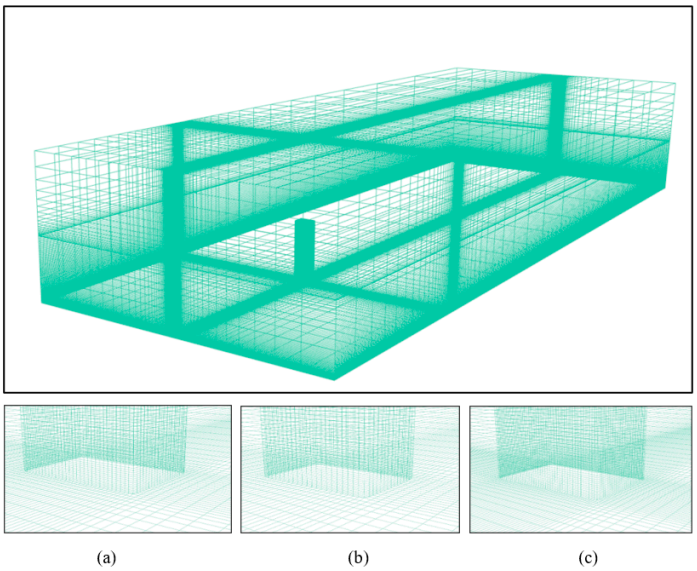

Figure 5. Mesh grid types: (**a**) coarse, (**b**) medium, (**c**) fine.

Table 2. Mesh resolutions and refinements.

Mesh Type	Coarse	Medium	Fine
Refinement	$(B/10)$	$(B/10) \times \sqrt{2}$	$(B/10) \times \sqrt{2} \times \sqrt{2}$
Grid Size (m)	2.16 m	1.52 m	1.08 m
Cell no.	196,460	285,120	445,312

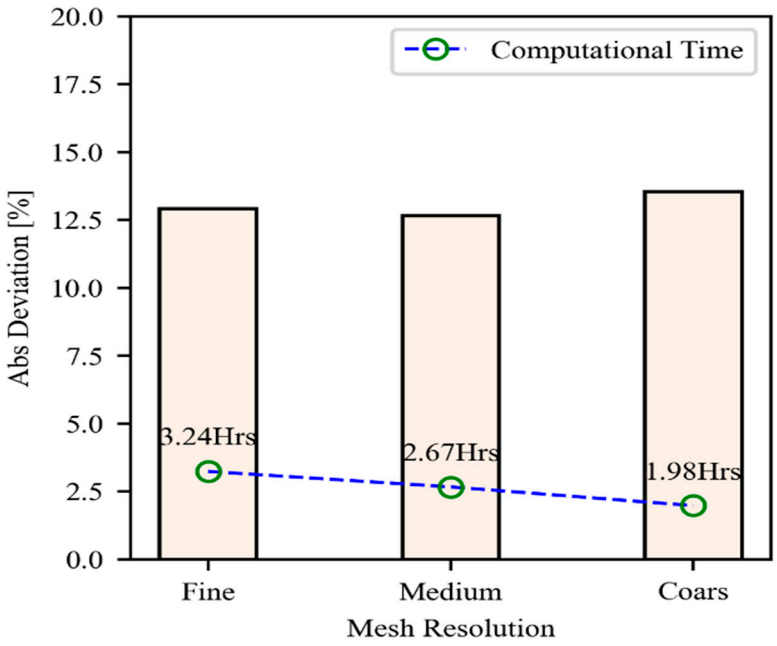

Figure 6. Absolute deviation of Cp for different mesh type.

3. Aerodynamic Optimization Procedure

Aerodynamic optimization is achieved by employing the surrogate RBF optimization algorithm. Different core processes are involved within every single round of this optimiza-

tion cycle, including computational fluid dynamics (CFD), fluid–structure interaction (FSI), and finite element analysis (FEA). The aerodynamic optimization process is then developed using the surrogate model technique with a radial basis function metamodel and includes all previous solvers and coupling within an optimization algorithm (Figure 7). The steps involved are illustrated and can be summarized as follows:

- Three-dimensional parametrical model reflecting the geometries of the building is created and design variables to be manipulated for aerodynamic modifications are identified.
- Design of experiment (DOE) is generated randomly within the design domain limit of the identified design variables.
- Objective function and its attributed limitations are constructed mathematically.
- Sampling points are then evaluated within the actual computationally expensive function (CFD-FSI-FEA) and interpolated against objective function to construct the surrogate model.
- Additional random sample point is introduced to the design space.
- Predicted value of the additional sample point is generated by the surrogate model, while its actual value is evaluated based on actual computational function (CFD-FSI-FEA)
- Root mean square error is computed for the additional sample point between the predicted and actual value. The additional sample point is added to the design space as training data, and the sampling point's k becomes k + 1.
- Steps 5 to 8 are repeated to refine the surrogate model until a zero to near-zero error value is achieved.
- The refined surrogate model is achieved where optimal function with its attributed design variables can be computed.
- Optimal design variables obtained from the surrogate model are evaluated based on actual function to further ensure its accuracy and confidence.

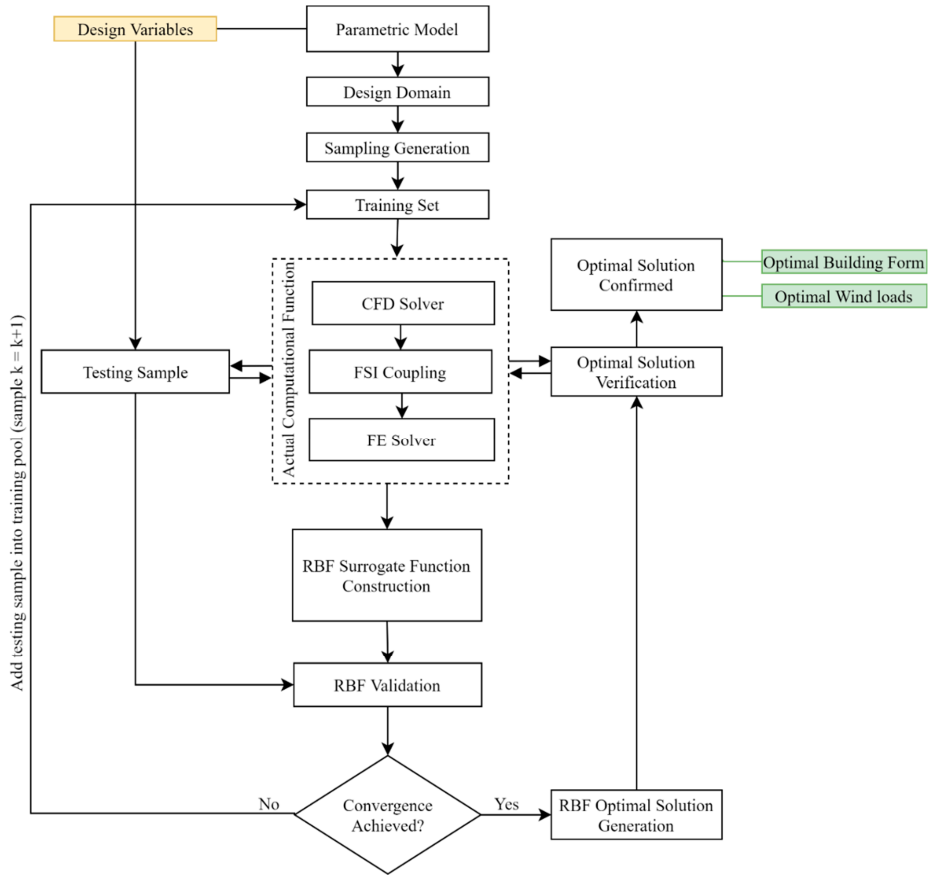

Figure 7. Aerodynamic optimization process.

4. Numerical Implementation

A case study: An existing irregular tall building project was chosen to implement the proposed optimization method and prove its feasibility and effectiveness. Cayan Tower in Dubai in Figure 8, the tallest twisting tower in the world, presents a good example of the current trend of complexity in tall building design. The tower is 306 m in height, with a spiral twisting shape of 90 degrees along its height, inspired by human DNA and designed by the SOM architectural group [40]. Although the twisting form is an effective major modification in reducing vortex-shedding dynamic responses of tall buildings in comparison to regular forms, the challenge remains by introducing minor aerodynamic modifications that preserve the design intent of the unique architectural and structural functions of this building to further optimize wind-induced loads with a less expensive and practical computational method.

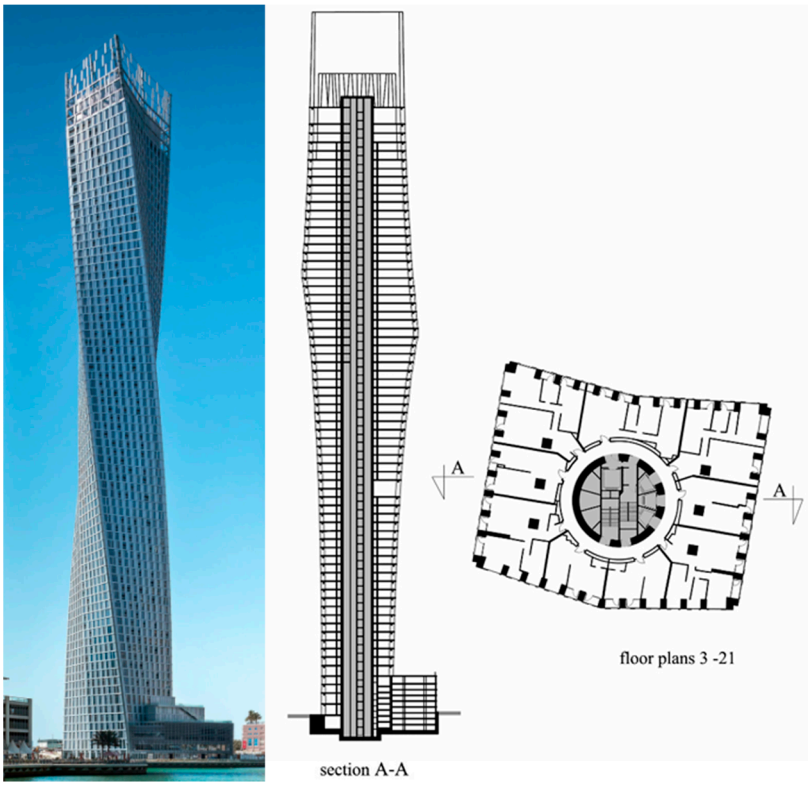

Figure 8. Cayan Tower, Dubai.

Based on the intensive literature presented above and the specific building configuration of this case study, two potential design variables are identified as minor modifications, which are corner rounding and building plan curvature. These two parameters allow for aerodynamic manipulation while preserving the global unique architectural form and structural function of the building. Edge corners are examined with rounding variation from 0 to max. 2 m fillet radius, while the building layout plan is modified by variation from 0 to max 10 degrees of curvature to its concave hexagon shape. The two design variables and their interval variations are illustrated in Figure 9.

Three inter-connected models were developed to carry out the aerodynamic optimization process as shown in Figure 10. A 3D bluff model representing the façade of the building was firstly created. Then, parametrical model reflecting the structural system of the building in reference to its architectural geometrical form was generated and transferred to a finite element model for structural assessment.

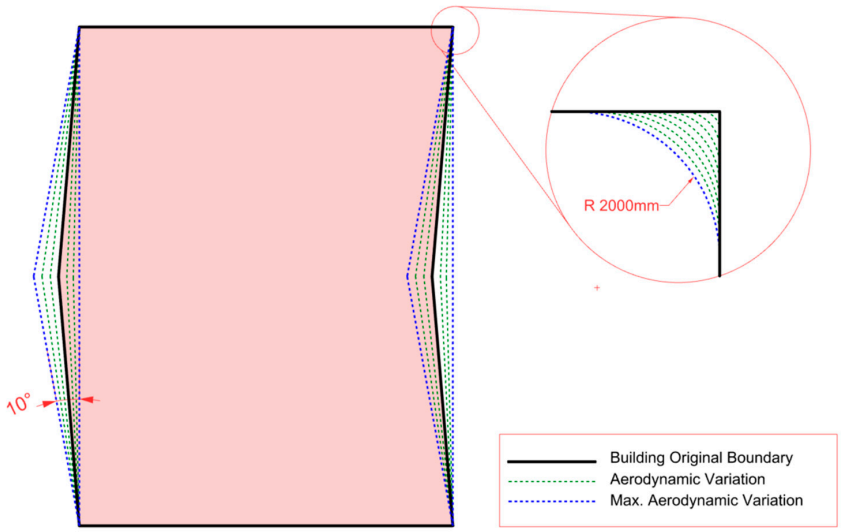

Figure 9. Aerodynamic modification parameters.

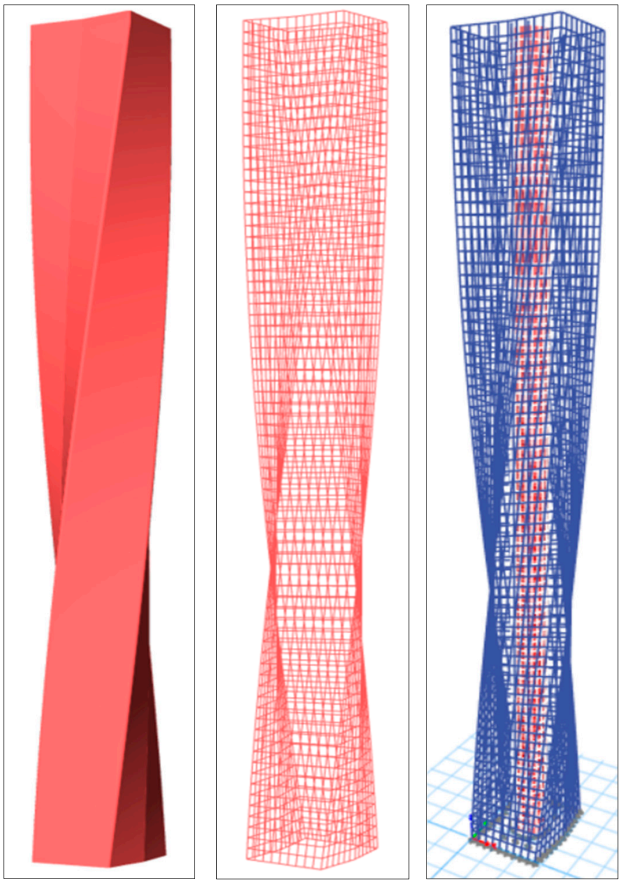

(**a**) (**b**) (**c**)

Figure 10. (**a**) Bluff model, (**b**) parametrical model, (**c**) structural Model.

4.1. RBF Surrogate Model

Surrogate model optimization is commonly used in CFD to take over the computationally expensive function evaluation with the inexpensive surrogate model representing the objective function in a given design space [41]. The Gaussian Radial Basis Function (RBF) was the appropriate surrogate model type chosen for this research based on several benchmark studies on optimization for architectural optimization problems [42].

4.1.1. Design of Experiment (DOE)

To generate the needed set of samples for the DOE, the Latin hypercube (LHC) technique was adopted. The benefit of such method over other similar methods of sampling is that it allows to create quasi-random samples across a multidimensional design space with fair distribution between the input variables domain [43]. A total of 10 sampling points were created through LHC and evaluated in CFD to develop an RBF surrogate model function, as illustrated in Figure 11.

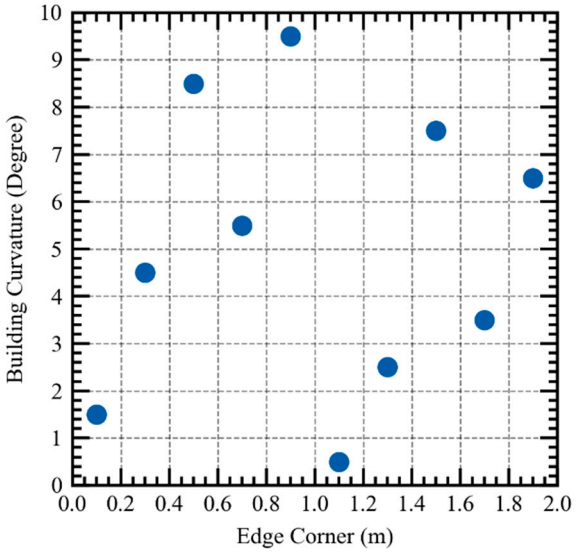

Figure 11. Sampling points.

4.1.2. CFD Process

A wind tunnel was created to evaluate sampling points against wind flow. Tunnel domain size was determined based on building height (H) with 2.3 m H, 10 H, 2.3 H, and 2.3 H for windward, leeward, sides, and top, respectively, as suggested by [38]. A blockage ratio of 1.05% was calculated through python script, ensuring it is below the endorsed block ratio of 5% [9]. Another script was developed to calculate mesh cell sizes relative to the building's dimension. A 2 m cell size was used as medium mesh regulation to balance between the accuracy of results and the computational time, as investigated in the CFD validation section. Figure 12 shows the virtual wind tunnel meshing.

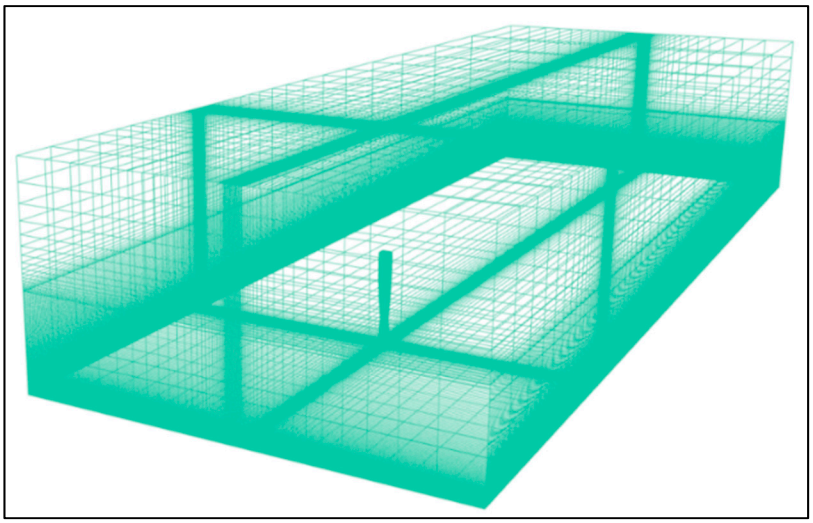

Figure 12. Virtual wind tunnel meshing.

4.1.3. FSI Coupling

The fluid–structure interaction (FSI) coupling algorithm was developed in python to translate the CFD output pressures into FE input loads. The translation procedure of FSI begins by converting the pressure exerted by the building façade mesh surfaces into vector forces with respect to surfaces' normals, as shown in Figure 13. Collected vectors are then consolidated horizontally and vertically for each story height to produce a single point load for X and Y directions, and a crossed product torsional moment is applied at the center of each story diaphragm. The total forces and moments for each sample point case study performed in CFD and transformed in FSI are represented in Figures 14 and 15.

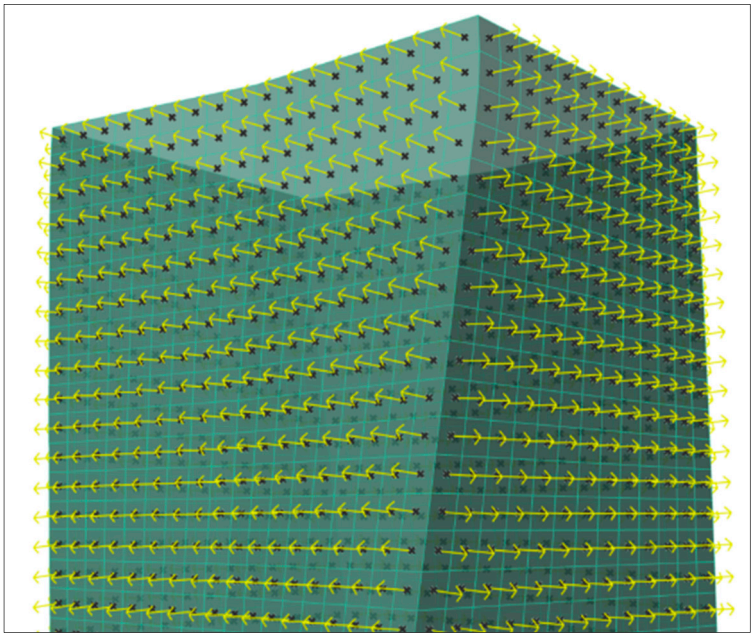

Figure 13. Building mesh faces and normal.

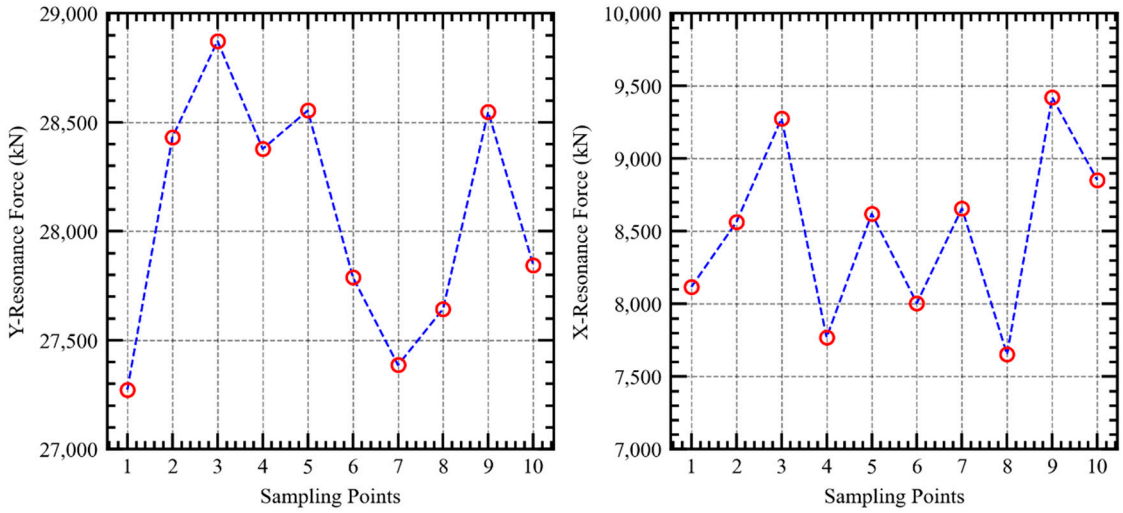

Figure 14. Along-wind and across-wind loads.

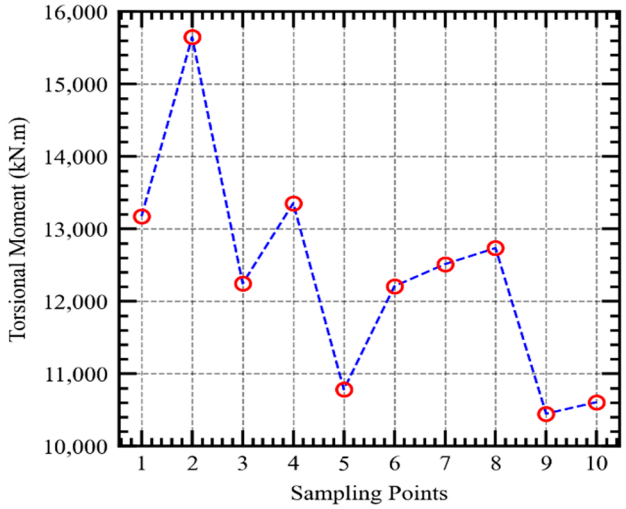

Figure 15. Torsional moment.

4.2. FE Analysis

In order to evaluate the structural response to wind action, the finite element analysis was carried out in ETABS [44] and python script was developed to interface with ETABS API and bridge FSI loads with FE analysis in an automotive process. Structural elements, including lateral resisting system, were all assumed based on the original design of the building and remain constant thorough the height of the structure. A rigid diaphragm was considered to ensure full translation of forces and displacements to the structural lateral system without deforming the contribution from slab stiffness. Forces were applied for each respective story to the center of the diaphragm that represents the center of mass in a given story, so that, in addition to the imposed torsional moment, eccentricity between the center of rigidity and center of mass is taken into account by FE analysis for torsional deformation. Figure 16 represents the maximum top structural deflections generated for each sampling point, while Figure 17 represents the maximum inter-story drifts. Table 3 summarizes the analysis of the ten sampling points according to their respective design variables.

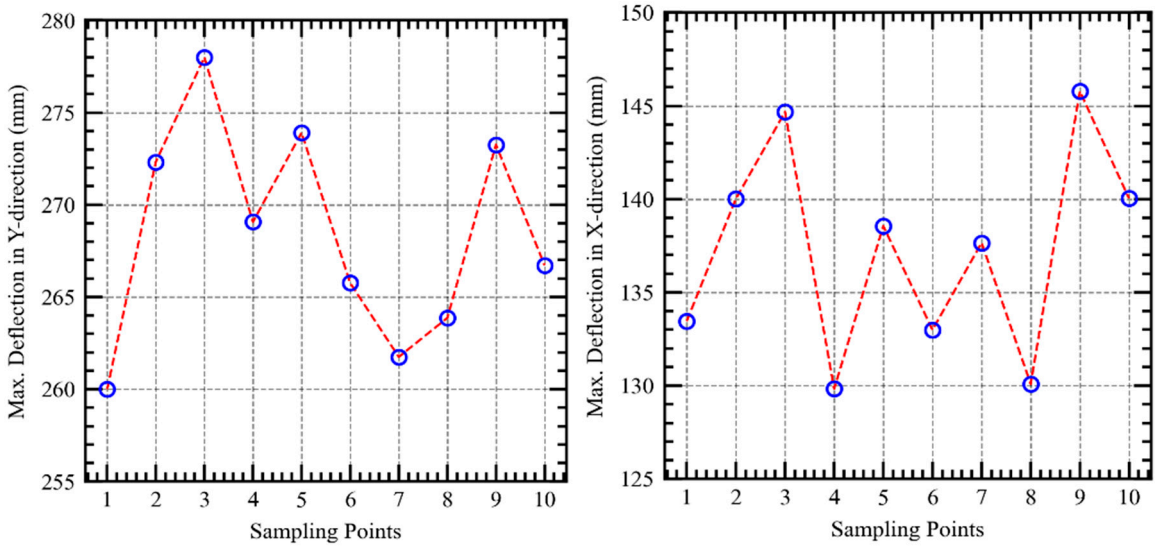

Figure 16. Maximum top structural deflection.

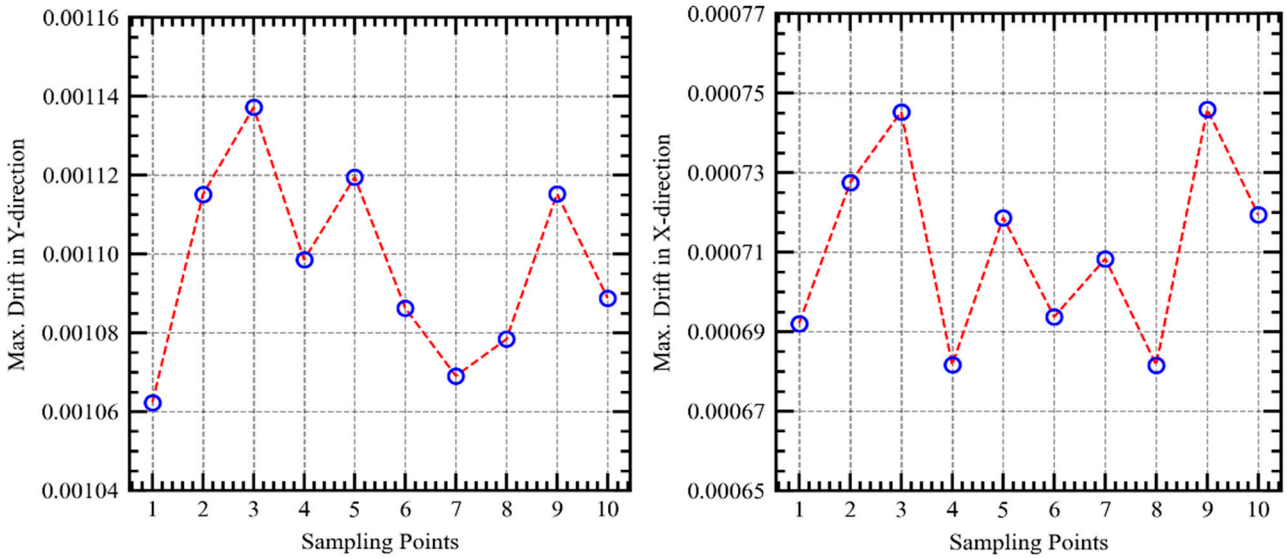

Figure 17. Maximum inter-story drifts.

Table 3. Sampling points evaluation summary.

Sample Points	Edge Curve	Building Curve	Fx	Fy	Mz	Def_x	Def_y	Drift_x	Drift_y
	(mm)	(Degree)	(kN)	(kN)	(kN m)	(mm)	(mm)	-	-
SP1	1.7	3.5	8116	27,273	13,177	133.46	260	0.000692	0.001062
SP2	0.3	4.5	8563	28,432	15,649	140.02	272.32	0.000727	0.001115
SP3	0.5	8.5	9277	28,873	12,247	144.68	278	0.000745	0.001137
SP4	0.1	1.5	7769	28,378	13,356	129.83	269.07	0.000682	0.001099
SP5	0.7	5.5	8621	28,554	10,782	138.56	273.91	0.000719	0.00112
SP6	1.3	2.5	8005	27,789	12,209	132.99	265.76	0.000694	0.001086
SP7	1.9	6.5	8658	27,386	12,514	137.66	261.75	0.000708	0.001069
SP8	1.1	0.5	7652	27,644	12,736	130.09	263.87	0.000682	0.001078
SP9	0.9	9.5	9422	28,548	10,449	145.79	273.26	0.000746	0.001115
SP10	1.5	7.5	8852	27,844	10,608	140.04	266.72	0.000719	0.001089

Objective Function

The aim of the objective function is to enhance structural performance due to wind-induced loads. Thus, the objective function in this study is to minimize the total deflection of the structure subjected to wind forces. Considering the complexity of the given geometrical form, and the FE results that demonstrated significant deflection values exerted in both x and y global directions, the objective function is then developed to minimize the resultant maximum deflection at the top of the structure. Considering the 2D design space domain constructed in this case study with $i = 1, 2, 3 \ldots$, N design variable vectors existing within the domain, and $j = 1, 2, 3 \ldots$, M stories, the objective function then can be mathematically expressed as:

$$\text{To minimize}: \ \hat{f}(a_i, b_i)\delta_{xy,top}$$

$$\text{Subject to}: \ \Delta_{y,\,j} \leq \Delta_{y,\,limit}; \Delta_{x,\,j} \leq \Delta_{x,\,limit}$$

$$a_i^L \leq a_i \leq a_i^U; \ b_i^L \leq b_i \leq b_i^U$$

where $\hat{f}(a_i, b_i)$ is the predicted RBF value for $\delta_{xy,\,top}$ which is the max resulted deflection in the x and y directions at the top of structure, a is the design variable for corner edge modification, b is the design variable for building curvature modification, L and U define the lower and upper bounds for the design variables, respectively, $\Delta_{y,\,j}$, $\Delta_{x,\,j}$ is the max story drift value in the y and x direction, and $\Delta_{y,\,limit}$, $\Delta_{x,\,limit}$ is the allowable limit as per a given standard; in this example, the Eurocode design code standard is adopted with a limit of H/500.

Four iterations with additional samples in each iteration were needed to converge the solution into an acceptable error margin, as shown in Table 4. The final constructed function is represented by the RBF surface response in Figure 18. It is observed from the RBF surface that potential optimal solutions can be obtained within the blue contours, which correspond to the maximum corner curving. In contrary, the opposite region with a minimum curving radius corresponds to maximum deflection values, and this evidence is supported by the fact that chamfering corners of building geometry can reduce wind loads on a structure significantly [4,5,45–48].

Table 4. RBF optimization summary.

No. Iterations	1	2	3	(Optimal)
No. Samples	11	12	13	14
Predicted (RBF)	305.62	297.61	298.50	283.61
Actual (CFD-FSI-FE)	311.44	296.62	298.71	283.87
RMSE (%)	5.82%	1.01%	0.20%	0.26%

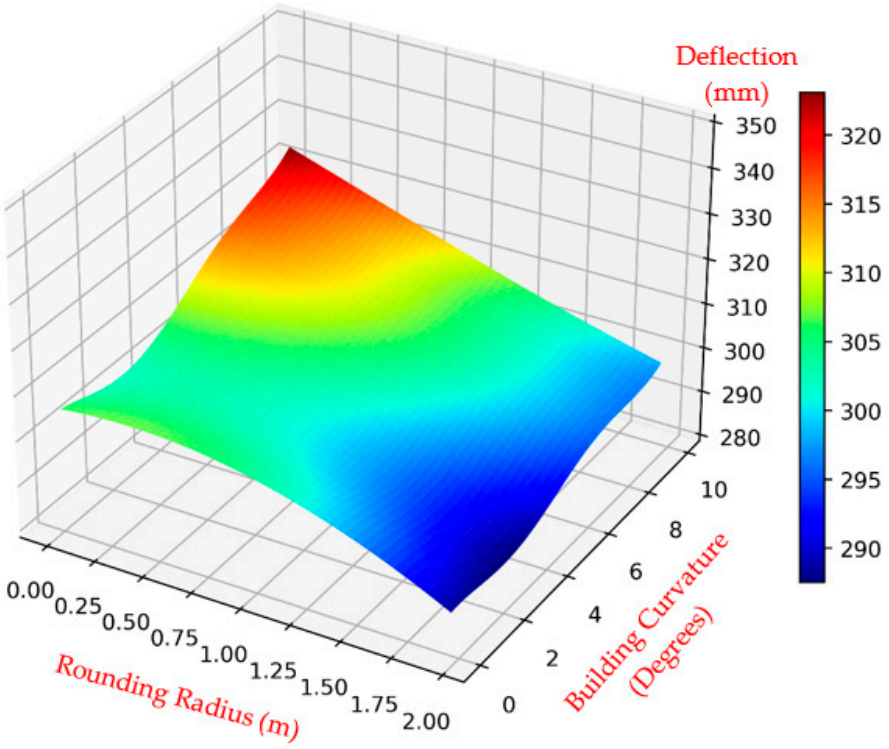

Figure 18. RBF response surface function.

One potential optimal solution for the modified building form is shown in Figure 19, illustrating the original and the new optimal boundaries of the aerodynamic modification applied through this optimization process. The new optimal boundary is obtained by reducing the original building curvature from 7° to 4° and chamfering the building sharp corner with a 2 m radius.

Comparison between original building form and new optimal form was conducted to evaluate the benefits of the proposed optimization methodology. Maximum deflection for both the optimal and original design is compared in Figure 20 for the along-wind and across-wind directions, respectively. In the along-wind direction, the optimal design was able to achieve a max deflection of 251.08 mm with a 12.95% reduction in comparison to the original of 288.45 mm. Similarly, in the across-wind direction the optimal design achieved a max deflection of 132.44 mm with a 14.53% reduction in comparison to the original design of 154.96 mm.

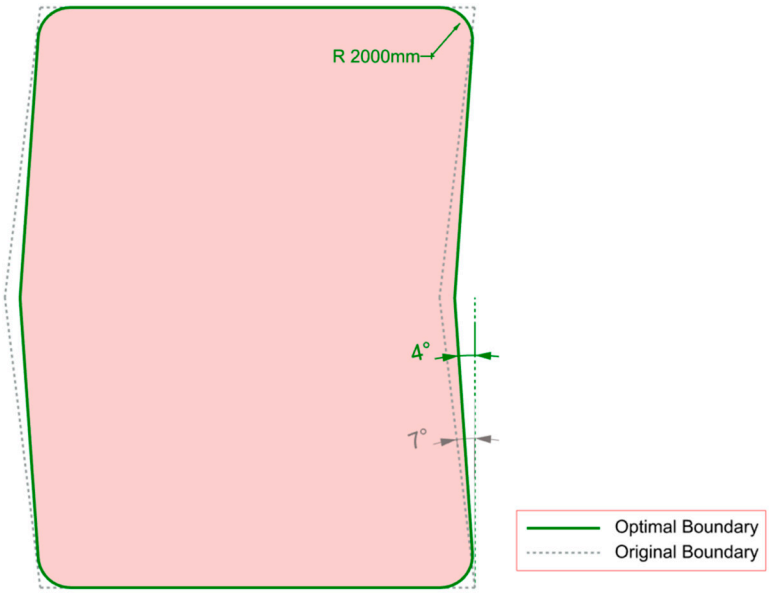

Figure 19. Optimal aerodynamic building layout.

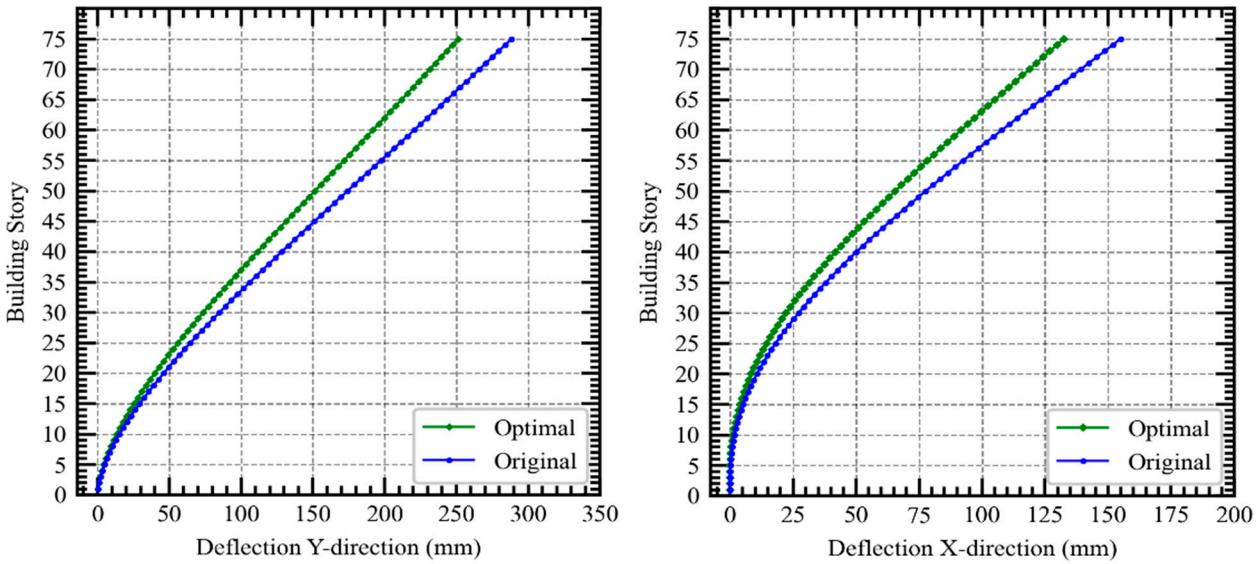

Figure 20. Maximum top structural deflection.

Inter-story drift for both the optimal and original design are compared and shown in Figure 21 for along-wind and across-wind directions, respectively. In the along-wind direction, it is observed that the max inter-story drifts occur in floors within the mid height of the structure, and the optimal design drift is reduced by 12.89% in comparison to the original. Similarly, in the across-wind direction, max drift occurs in floors near the top height of the structure, and optimal design drift is reduced by 13.45% from original one.

Finally, the aerodynamic optimal loads are compared to wind loads for original building geometry. Figure 22 represents the generated forces by CFD in along-wind and across-wind directions, respectively, where for the along-wind direction the total optimal loads are less by 4173 kN in comparison to the original shape, with a reduction percentage of 13.83%. Similarly, for the across-wind direction, the total optimal loads are less by 2340 kN from original shape, with a reduction percentage of 23.12%. The considerable change in wind load magnitude by employing the developed computational method and through manipulation of building geometrical forms opens wide opportunities that are not

limited to minimizing loads and their structural response on tall buildings, but also for employing these loads for wind energy harvesting to produce sustainable green power.

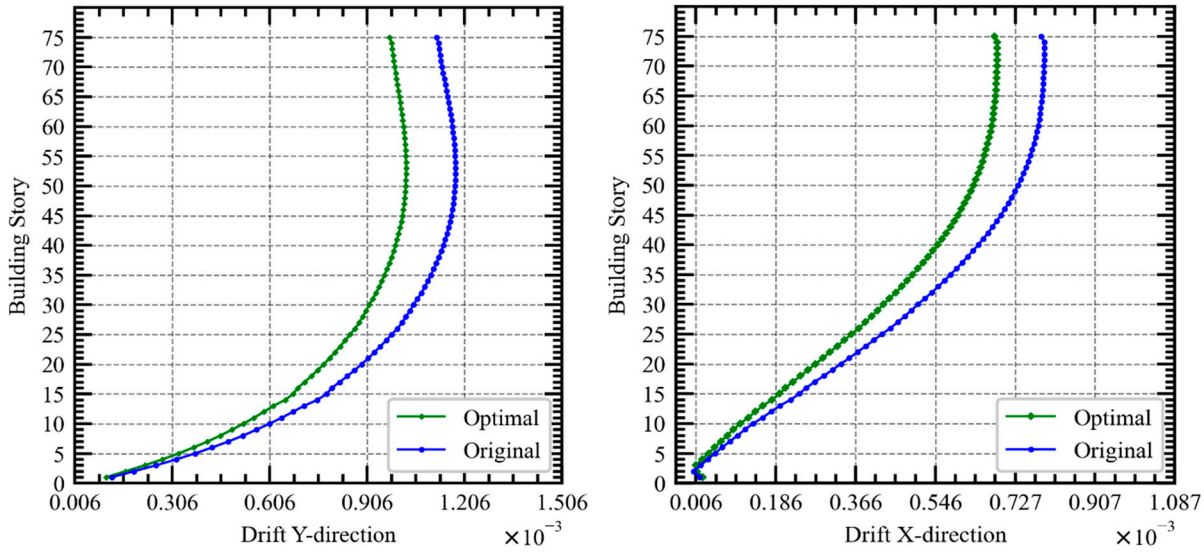

Figure 21. Maximum inter-story drifts.

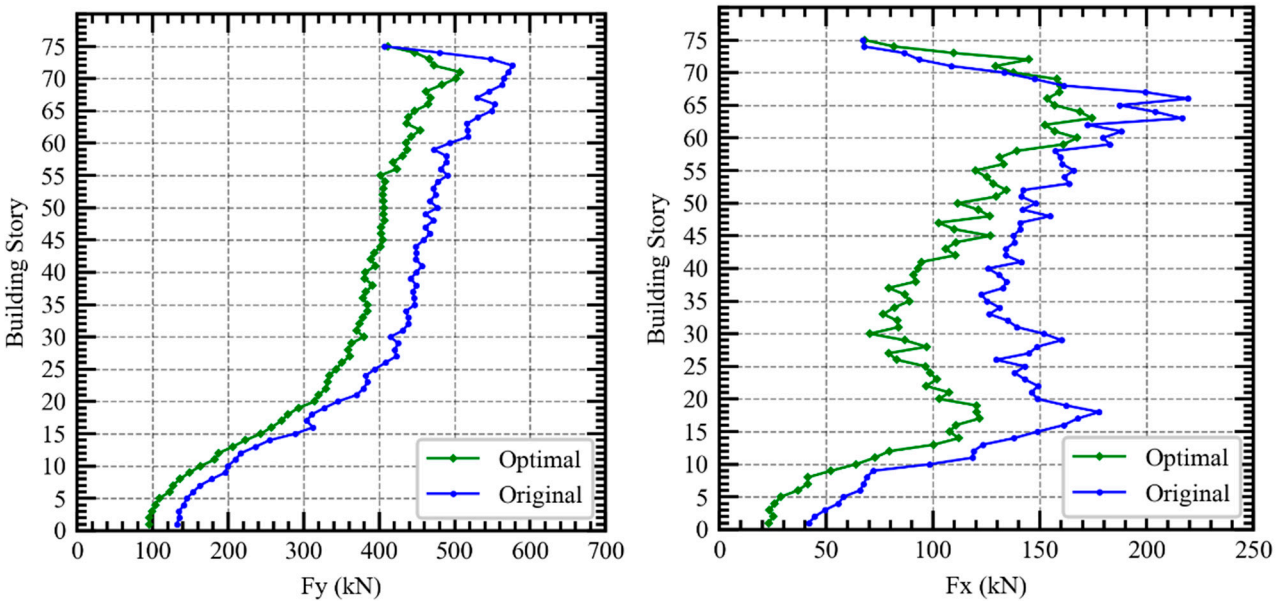

Figure 22. Imposed wind loads on building.

5. Conclusions

It can be satisfactory concluded that the adopted approach proved its effectiveness in optimizing wind loads on a complex tall structure, and consequently the structural response represented by deflection and drift is also minimized. The computational tools developed in the study, by integrating a parametric model, computational fluid dynamics, fluid–dynamic interaction, and structural finite element analysis, showed its capability and effectiveness to optimize a tall building aerodynamically. The case study implemented in this research work was a 75-story (300 m in height) building with a complex geometrical shape (twisting form), and the developed approach and tools were able to mitigate the impact of wind loads on the structure by manipulating the layout of the building with only minor modifications that have little to no impact on the original architectural and structural design. From the studied example, the following conclusions can be deduced:

- Although only one wind direction was considered in this study, the results showed an effective minimization of structural responses on both along-wind and across-wind directions.
- The translated percentage of reduction in top structural deflection for both along-wind and across-wind are 12.95% and 14.53%, respectively.
- The translated percentage of reduction in inter-story drift for both along-wind and across-wind are 12.89% and 13.54%, respectively.
- The translated percentage of reduction in imposed wind loads for both along-wind and across-wind are 13.83% and 23.12%, respectively.
- The development of the surrogate model function showed to be effective in estimating highly non-linear functions in the case of large architectural problems.
- The efficiency of aerodynamic optimization together with the capability of computational tools are expected to encourage both architects and engineers to employ them while seeking better decisions at preliminary design stages.
- Adopting computational methods that integrate the requirements of both architects and engineers, as well as the evaluation with full interaction in a single virtual environment similar to what is presented in this paper, allows for a multidisciplinary design approach and connects both professions in more integrated manner.

Future studies shall be extended by integrating another level of lateral structural system optimization together with aerodynamic optimization. Thus, when considering structural optimization, both static and dynamic response of the building shall be taken into account for measuring structural responses.

Author Contributions: Conceptualization, F.A., N.K., W.I.G. and N.S.; Data curation, F.A., N.K., W.I.G., N.S., M.A., E.V.K. and M.A.A.; Formal analysis, F.A., N.K., W.I.G., N.S., M.A., E.V.K. and M.A.A.; Funding acquisition, M.A. and E.V.K.; Investigation, F.A. and M.A.A.; Methodology, F.A., N.K. and W.I.G.; Resources, F.A., N.K., W.I.G., N.S., M.A., E.V.K. and M.A.A.; Software, F.A. and M.A.A.; Supervision, N.K., W.I.G. and N.S.; Validation, N.K., W.I.G., N.S., M.A., E.V.K. and M.A.A.; Visualization, F.A., M.A. and E.V.K.; Writing—original draft, F.A.; Writing—review and editing, N.K., W.I.G., N.S., M.A., E.V.K. and M.A.A. All authors have read and agreed to the published version of the manuscript.

Funding: The research is partially funded by the Ministry of Science and Higher Education of the Russian Federation as part of the World-class Research Center program: Advanced Digital Technologies (contract No. 075-15-2022-311, dated 20 April 2022).

Institutional Review Board Statement: Not applicable.

Informed Consent Statement: Not applicable.

Data Availability Statement: Not applicable.

Acknowledgments: This research was supported by the faculty of Civil Engineering and Built Environment, Universiti Tun Hussein Onn Malaysia (UTHM), Johor, Malaysia. Also, the authors gratefully acknowledge the financial support given by the Deanship of Scientific Research at Prince Sattam bin Abdulaziz University, Alkharj, Saudi Arabia, for this research.

Conflicts of Interest: The authors declare no conflict of interest.

References

1. Oldfield, P. *The Sustainable Tall Building: A Design Primer*; Routledge: London, UK, 2019.
2. Alkhatib, F.; Kasim, N.; Goh, W.I.; Al-masudi, A. Multidisciplinary Computational Optimization: An Integrated Approach to Achieve Sustainability in Tall Building Design at Early Stage-Review. In Proceedings of the 2021 Third International Sustainability and Resilience Conference: Climate Change, Sakheer, Bahrain, 15–16 November 2021; IEEE: Piscataway, NJ, USA, 2021; pp. 562–566.
3. Hamidavi, T.; Abrishami, S.; Hosseini, M.R. Towards intelligent structural design of buildings: A BIM-based solution. *J. Build. Eng.* **2020**, *32*, 101685. [CrossRef]
4. Elshaer, A.; Bitsuamlak, G.; El Damatty, A. Enhancing wind performance of tall buildings using corner aerodynamic optimization. *Eng. Struct.* **2017**, *136*, 133–148. [CrossRef]

5. Sharma, A.; Mittal, H.; Gairola, A. Mitigation of wind load on tall buildings through aerodynamic modifications: Review. *J. Build. Eng.* **2018**, *18*, 180–194. [CrossRef]
6. Hayashida, H.; Iwasa, Y. Aerodynamic shape effects of tall building for vortex induced vibration. *J. Wind Eng. Ind. Aerodyn.* **1990**, *33*, 237–242. [CrossRef]
7. Kim, Y.; Tamura, Y.; Tanaka, H.; Ohtake, K.; Bandi, E.; Yoshida, A. Wind-induced responses of super-tall buildings with various atypical building shapes. *J. Wind Eng. Ind. Aerodyn.* **2014**, *133*, 191–199. [CrossRef]
8. Bhattacharyya, B.; Dalui, S.K.; Ahuja, A.K. Wind induced pressure on 'E'plan shaped tall buildings. *Jordan J. Civ. Eng.* **2014**, *8*, 120.
9. Mou, B.; He, B.-J.; Zhao, D.-X.; Chau, K.-W. Numerical simulation of the effects of building dimensional variation on wind pressure distribution. *Eng. Appl. Comput. Fluid Mech.* **2017**, *11*, 293–309. [CrossRef]
10. Paul, R.; Dalui, S. Shape optimization to reduce wind pressure on the surfaces of a rectangular building with horizontal limbs. *Period. Polytech. Civ. Eng.* **2021**, *65*, 134–149. [CrossRef]
11. Kim, Y.-M.; You, K.-P. Dynamic responses of a tapered tall building to wind loads. *J. Wind Eng. Ind. Aerodyn.* **2002**, *90*, 1771–1782. [CrossRef]
12. Kim, Y.-M.; You, K.-P.; Ko, N.-H. Across-wind responses of an aeroelastic tapered tall building. *J. Wind Eng. Ind. Aerodyn.* **2008**, *96*, 1307–1319. [CrossRef]
13. Xie, J. Aerodynamic optimization of super-tall buildings and its effectiveness assessment. *J. Wind Eng. Ind. Aerodyn.* **2014**, *130*, 88–98. [CrossRef]
14. Bairagi, A.K.; Dalui, S.K. *Advances in Structures, Systems and Materials*; Springer: Singapore, 2020; pp. 31–38.
15. Bairagi, A.K.; Dalui, S.K. Comparison of aerodynamic coefficients of setback tall buildings due to wind load. *Asian J. Civ. Eng.* **2018**, *19*, 205–221. [CrossRef]
16. Dutton, R.; Isyumov, N. Reduction of tall building motion by aerodynamic treatments. *J. Wind Eng. Ind. Aerodyn.* **1990**, *36*, 739–747. [CrossRef]
17. Ruiz, C.A.; Kalkman, I.; Blocken, B. Aerodynamic design optimization of ducted openings through high-rise buildings for wind energy harvesting. *Build. Environ.* **2021**, *202*, 108028. [CrossRef]
18. Tamura, T.; Miyagi, T.; Kitagishi, T. Numerical prediction of unsteady pressures on a square cylinder with various corner shapes. *J. Wind Eng. Ind. Aerodyn.* **1998**, *74*, 531–542. [CrossRef]
19. Miyashita, K.; Katagiri, J.; Nakamura, O.; Ohkuma, T.; Tamura, Y.; Itoh, M.; Mimachi, T. Wind-induced response of high-rise buildings effects of corner cuts or openings in square buildings. *J. Wind Eng. Ind. Aerodyn.* **1993**, *50*, 319–328. [CrossRef]
20. Kwok, K. Effect of building shape on wind-induced response of tall building. *J. Wind Eng. Ind. Aerodyn.* **1988**, *28*, 381–390. [CrossRef]
21. Tamura, T.; Miyagi, T. The effect of turbulence on aerodynamic forces on a square cylinder with various corner shapes. *J. Wind Eng. Ind. Aerodyn.* **1999**, *83*, 135–145. [CrossRef]
22. Tse, K.-T.; Hitchcock, P.A.; Kwok, K.C.; Thepmongkorn, S.; Chan, C.M. Economic perspectives of aerodynamic treatments of square tall buildings. *J. Wind Eng. Ind. Aerodyn.* **2009**, *97*, 455–467. [CrossRef]
23. Zhengwei, Z.; Yonga, Q.; Minga, G.; Nankuna, T.; Yongc, X. Effects of corner recession modification on aerodynamic coefficients of square tall buildings. In Proceedings of the Seventh International Colloquium on Bluff Body Aerodynamics and Applications, Shanghai, China, 2–6 September 2012.
24. Li, Y.; Tian, X.; Tee, K.F.; Li, Q.-S.; Li, Y.-G. Aerodynamic treatments for reduction of wind loads on high-rise buildings. *J. Wind Eng. Ind. Aerodyn.* **2018**, *172*, 107–115. [CrossRef]
25. Thordal, M.S.; Bennetsen, J.C.; Capra, S.; Kragh, A.K.; Koss, H.H.H. Towards a standard CFD setup for wind load assessment of high-rise buildings: Part 2—Blind test of chamfered and rounded corner high-rise buildings. *J. Wind Eng. Ind. Aerodyn.* **2020**, *205*, 104282. [CrossRef]
26. Mandal, S.; Dalui, S.K.; Bhattacharjya, S. Wind induced response of corner modified 'U' plan shaped tall building. *Wind. Struct.* **2021**, *32*, 521–537.
27. Kwok, K.C.; Bailey, P.A. Aerodynamic devices for tall buildings and structures. *J. Eng. Mech.* **1987**, *113*, 349–365. [CrossRef]
28. Gaur, N.; Raj, R. Aerodynamic mitigation by corner modification on square model under wind loads employing CFD and wind tunnel. *Ain Shams Eng. J.* **2022**, *13*, 101521. [CrossRef]
29. Sanyal, P.; Dalui, S.K. Forecasting of aerodynamic coefficients of tri-axially symmetrical Y plan shaped tall building based on CFD data trained ANN. *J. Build. Eng.* **2022**, *47*, 103889. [CrossRef]
30. Gu, M.; Quan, Y. Across-wind loads of typical tall buildings. *J. Wind Eng. Ind. Aerodyn.* **2004**, *92*, 1147–1165. [CrossRef]
31. Tanaka, H.; Tamura, Y.; Ohtake, K.; Nakai, M.; Kim, Y.C. Experimental investigation of aerodynamic forces and wind pressures acting on tall buildings with various unconventional configurations. *J. Wind Eng. Ind. Aerodyn.* **2012**, *107*, 179–191. [CrossRef]
32. Tamura, Y.; Kim, Y.; Tanaka, H.; Bandi, E.; Yoshida, A.; Ohtake, K. Aerodynamic and response characteristics of super-tall buildings with various configurations. In Proceedings of the 8th Asia-Pacific Conference on Wind Engineering, Chennai, India, 10–14 December 2013.
33. Baghaei Daemei, A.; Mehrinejad Khotbehsara, E.; Malekian, E.; Bahrami, P. Study on wind aerodynamic and flow characteristics of triangular-shaped tall buildings and CFD simulation in order to assess drag coefficient. *Ain Shams Eng. J.* **2019**, *10*, 541–548. [CrossRef]
34. Assainar, N.; Dalui, S.K. Aerodynamic analysis of pentagon-shaped tall buildings. *Asian J. Civ. Eng.* **2021**, *22*, 33–48. [CrossRef]

35. Huang, M.; Li, Q.; Chan, C.M.; Lou, W.; Kwok KC, S.; Li, G. Performance-based design optimization of tall concrete framed structures subject to wind excitations. *J. Wind Eng. Ind. Aerodyn.* **2015**, *139*, 70–81. [CrossRef]
36. Melbourne, W. Comparison of measurements on the CAARC standard tall building model in simulated model wind flows. *J. Wind Eng. Ind. Aerodyn.* **1980**, *6*, 73–88. [CrossRef]
37. Meng, F.-Q.; He, B.-J.; Zhu, J.; Zhao, D.-X.; Darko, A.; Zhao, Z.-Q. Sensitivity analysis of wind pressure coefficients on CAARC standard tall buildings in CFD simulations. *J. Build. Eng.* **2018**, *16*, 146–158. [CrossRef]
38. Franke, J.; Hellsten, A.; Schlünzen, K.; Carissimo, B. Best practice guideline for the CFD simulation of flows in the urban environment-a summary. In Proceedings of the 11th Conference on Harmonisation within Atmospheric Dispersion Modelling for Regulatory Purposes, Cambridge, UK, 2–5 July 2007; Cambridge Environmental Research Consultants: Cambridge, UK, 2007.
39. Zhao, D.-X.; He, B.-J. Effects of architectural shapes on surface wind pressure distribution: Case studies of oval-shaped tall buildings. *J. Build. Eng.* **2017**, *12*, 219–228. [CrossRef]
40. Golasz-Szolomicka, H.; Szolomicki, J. Architectural and structural analysis of selected twisted tall buildings. *IOP Conf. Ser. Mater. Sci. Eng.* **2019**, *471*, 052050. [CrossRef]
41. Moore, W.O.W.; Mala-Jetmarova, H.; Gebreslassie, M.; Tabor, G.R.; Belmont, M.R.; Savic, D.A. Comparison of multiple surrogates for 3D CFD model in tidal farm optimisation. *Procedia Eng.* **2016**, *154*, 1132–1139. [CrossRef]
42. Wortmann, T. Opossum-introducing and evaluating a model-based optimization tool for grasshopper. In Proceedings of the 22nd International Conference of the Association for Computer-Aided Architectural Design Research in Asia (CAADRIA), Hong Kong, 5–8 April 2017.
43. Navid, A.; Khalilarya, S.; Abbasi, M. Diesel engine optimization with multi-objective performance characteristics by non-evolutionary Nelder-Mead algorithm: Sobol sequence and Latin hypercube sampling methods comparison in DoE process. *Fuel* **2018**, *228*, 349–367. [CrossRef]
44. Habibullah, A. *ETABS Nonlinear, Three Dimensional Analysis and Design of Building Systems*; Computer and Structures, Inc.: Berkeley, CA, USA, 1998.
45. Mooneghi, M.A.; Kargarmoakhar, R. Aerodynamic Mitigation and Shape Optimization of Buildings: Review. *J. Build. Eng.* **2016**, *6*, 225–235. [CrossRef]
46. Auwalu, A.S.; Noor, N.; Shazwan, M.; Shah, A.; Umar, S.; Amran, M.; Adamu, M.; Vatin, N.I.; Fediuk, R. Performance of Steel-Bolt-Connected Industrialized Building System Frame Subjected to Hydrodynamic Force. *Appl. Sci.* **2022**, *12*, 5093. [CrossRef]
47. Yip, C.C.; Wong, J.Y.; Amran, M.; Fediuk, R.; Vatin, N.I. Reliability Analysis of Reinforced Concrete Structure with Shock Absorber Damper under Pseudo-Dynamic Loads. *Materials* **2022**, *15*, 2688. [CrossRef]
48. Yip, C.C.; Marsono, A.K.; Wong, J.Y.; Amran, M.Y.H. Flexural strength of special reinforced lightweight concrete beam for Industrialised Building System (IBS). *J. Teknol.* **2015**, *77*, 187–196. [CrossRef]